INVERSE PROBLEM OF AN EMBEDDED METALLIC CYLINDER

Wei Chien, Chien-Ching Chiu and Chung-Hsin Huang

Electrical Engineering Department, Tamkang University
Tamsui, Taiwan, R.O.C
Phone:+886226215656 # 2737 Fax: +886226209814 e-mail:chiu@ee.tku.edu.tw

Abstract. In this paper we address an inverse scattering problem whose aim is to discuss the CPU time for recovering a perfectly conducting cylindrical object buried in a slab medium. First, we use Fourier-series or cubic-spline methods to describe the shape and reformulate the inverse problem into an optimization one. Then we solved it by the improved Steady State Genetic Algorithm (SSGA) with different crossover rate and Simple Genetic Algorithm (SGA) respectively and compare the cost time in finding out the global extreme solution of the objective function. It is found the searching ability of SSGA is much powerful than that of the SGA. Numerical results are given to show that the imaging problem by using SSGA is much better than SGA in time costing.

Introduction

The electromagnetic imaging of objects buried in a slab medium has attracted considerable attention in with a large potential impact on geosciences and remote sensing and pipelines applications in recent years [1]. However, the solutions are considerably more difficult than those involving objects in a free space and half space. This is due to the interaction between the interface of the three layers and the object, which leads to the complicated Green's function for this three layer problem. The GA [1]-[3] is an evolutionary algorithm that uses the stochastic mechanism to search through the parameter space. As compared to the gradient-based searching techniques, the genetic algorithm is less prone to converge to a local extreme. In this paper, inverse problem of the slab medium case solved by an improved SSGA using non-uniform probability density function (pdf) is proposed and compared with SGA.

Theoretical Formulation

Let us consider a two-dimensional slab structure as shown in Fig. 1, where (ε_i, σ_i) $i = 1,2,3$, denote the permittivities and conductivities in each region. Here the permeabilities of all three regions are assumed to be μ_o and a conducting cylinder is buried in region 2. The metallic cylinder with cross section described by the equation $\rho = F(\theta)$ is illuminated by an incident plane wave whose electric field vector is parallel to the Z axis (i.e., TM polarization). We assume that the time dependence of the field is harmonic with the factor $\exp(j\omega t)$. Let E_{inc} denote the incident field form region 1 with incident angle θ_1 as follow:

$$E_{inc} = E_1^+ e^{+jk_1 \cos\theta_1 y} e^{-jk_1 \sin\theta_1 x} \hat{z} \qquad (1)$$

Owing to the interfaces, the incident plane wave generates three waves that would exist in the absence of the conducting object. Thus, the unperturbed field is given by

$$E = \begin{cases} E_1 = E_1^+ e^{+jk_1\cos\theta_1 y} e^{-jk_1\sin\theta_1 x}\hat{z} \\ \qquad + E_1^- e^{-jk_1\cos\theta_1 y} e^{-jk_1\sin\theta_1 x}\hat{z} \quad , y \geq a \\ E_2 = E_2^+ e^{+jk_2\cos\theta_2 y} e^{-jk_2\sin\theta_2 x}\hat{z} \\ \qquad + E_2^- e^{-jk_2\cos\theta_2 y} e^{-jk_{21}\sin\theta_2 x}\hat{z}, \quad a \geq y \geq -a \\ E_3 = E_3^+ e^{+jk_3\cos\theta_3 y} e^{-jk_3\sin\theta_3 x}\hat{z}, \quad y \leq -a \end{cases} \qquad (2)$$
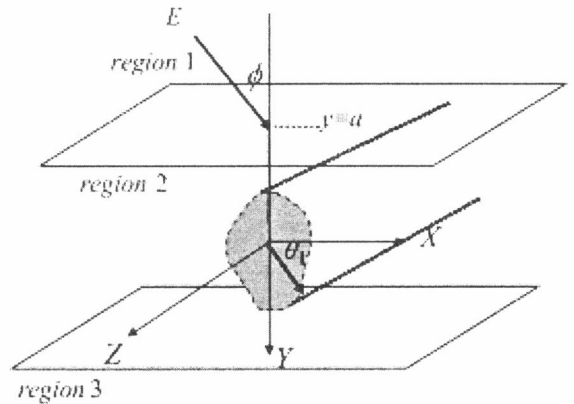
where the E_1^+ is set to be 1 and

Fig. 1 Geometry of the problem in (x,y) plane

$$E_1^- = \frac{e^{+j2k_1\cos\theta_1 a}[(Z_1 + Z_2)(Z_3 - Z_2)e^{-j2k_2\cos\theta_2 a} - (Z_1 - Z_2)(Z_3 + Z_2)e^{+j2k_2\cos\theta_2 a}]}{(Z_1 + Z_2)(Z_3 + Z_2)e^{+j2k_2\cos\theta_2 a} - (Z_1 - Z_2)(Z_3 - Z_2)e^{-j2k_2\cos\theta_2 a}}$$

$$E_2^+ = \frac{1}{2}e^{-jk_2\cos\theta_2 a}\left(\frac{Z_1+Z_2}{Z_1}e^{jk_1\cos\theta_1 a} + \frac{Z_1-Z_2}{Z_1}E_1^- e^{-jk_1\cos\theta_1 a}\right)$$

$$E_2^- = \frac{1}{2}e^{jk_2\cos\theta_2 a}\left(\frac{Z_1-Z_2}{Z_1}e^{jk_1\cos\theta_1 a} + \frac{Z_1+Z_2}{Z_1}E_1^- e^{-jk_1\cos\theta_1 a}\right) \qquad E_3^+ = \frac{2Z_3}{Z_2+Z_3}E_2^+ e^{(jk_3\cos\theta_3 a - jk_2\cos\theta_2 a)}$$

$$k_1\sin\theta_1 = k_2\sin\theta_2 = k_3\sin\theta_3, k_i^2 = \omega^2\varepsilon_i\mu_0 - j\omega\mu_0\sigma_i, \ i=1,2,3 \qquad \mathrm{Im}(k_i) \le 0$$

$$Z_1 = \frac{\eta_1}{\cos\theta_1}, Z_2 = \frac{\eta_2}{\cos\theta_2}, Z_3 = \frac{\eta_3}{\cos\theta_3} \qquad ,\eta_1 = \sqrt{\frac{\mu_0}{\varepsilon_1}}, \eta_2 = \sqrt{\frac{\mu_0}{\varepsilon_2}}, \eta_3 = \sqrt{\frac{\mu_0}{\varepsilon_3}}$$

At an arbitrary point (x,y) (or (r,θ) in polar coordinates) in regions 1 and 3 the scattered field, $\bar{E}_s = \bar{E} - \bar{E}_i$, can be expressed as

$$E_s(\bar{r}) = -\int_0^{2\pi} G(\bar{r}, F(\theta'),\theta')J(\theta')d\theta' \qquad (3)$$

where $J(\theta) = -j\omega\mu_0\sqrt{F^2(\theta)+F'^2(\theta)}J_s(\theta)$, $F(\theta)$ is the shape function and $F'(\theta)$ is the differentiation of $F(\theta)$. and

$$G(x,y;x',y') = \begin{cases} G_1(x,y;x',y'), & y > a \\ G_2(x,y;x',y'), & a > y > -a \\ G_3(x,y;x',y'), & y < -a \end{cases} \qquad (4)$$

$$G_1 = \frac{1}{2\pi}\int_{-\infty}^{\infty} je^{-j\gamma_1(y-a)}\frac{(\gamma_2+\gamma_3)e^{j\gamma_2(y'+a)}+(\gamma_2-\gamma_3)e^{-j\gamma_2(y'+a)}}{(\gamma_1+\gamma_2)(\gamma_2+\gamma_3)e^{j\gamma_2(2a)}+(\gamma_1-\gamma_2)(\gamma_2-\gamma_3)e^{-j\gamma_2(2a)}}e^{-j\alpha(x-x')}d\alpha$$

$$G_2 = \frac{1}{2\pi}\int_{-\infty}^{\infty}\frac{j}{2\gamma_2}\{[\frac{(\gamma_1+\gamma_2)(\gamma_2+\gamma_3)e^{-j\gamma_2[|y-y'|-2a]}+(\gamma_2-\gamma_1)(\gamma_2-\gamma_3)e^{j\gamma_2[|y-y'|-2a]}}{(\gamma_1+\gamma_2)(\gamma_2+\gamma_3)e^{j\gamma_2(2a)}+(\gamma_1-\gamma_2)(\gamma_2-\gamma_3)e^{-j\gamma_2(2a)}}]+$$

$$[\frac{(\gamma_2-\gamma_1)(\gamma_2+\gamma_3)e^{j\gamma_2[y+y']}+(\gamma_2-\gamma_3)(\gamma_1+\gamma_2)e^{-j\gamma_2[y+y']}}{(\gamma_1+\gamma_2)(\gamma_2+\gamma_3)e^{j\gamma_2(2a)}+(\gamma_1-\gamma_2)(\gamma_2-\gamma_3)e^{-j\gamma_2(2a)}}]\}e^{-j\alpha(x-x')}d\alpha$$

$$G_3 = \frac{1}{2\pi}\int_{-\infty}^{\infty}je^{j\gamma_3(y+a)}(\frac{(\gamma_1+\gamma_2)e^{-j\gamma_2(y'-a)}+(\gamma_2-\gamma_1)e^{j\gamma_2(y'-a)}}{(\gamma_1+\gamma_2)(\gamma_2+\gamma_3)e^{j\gamma_2(2a)}+(\gamma_1-\gamma_2)(\gamma_2-\gamma_3)e^{-j\gamma_2(2a)}}e^{-j\alpha(x-x')}d\alpha$$

with $\gamma_i^2 = k_i^2 - \alpha^2, i=1,2,3,$, and $\mathrm{Im}(\gamma_i) \le 0$

Note that G_1, G_2 and G_3 denote the Green's function which can be obtained by tedious mathematic manipulation for the line source in region 2. $J_s(\theta)$ is the induced surface current density, which is proportional to the normal derivative of the electric field on the conductor surface. The boundary condition on the surface of the scatterer states that the total tangential electrical field must be zero and yield an integral equation for $J(\theta)$:

$$E_2(\bar{r}) = -\int_0^{2\pi} G_2(\bar{r}, F(\theta'),\theta')J(\theta')d\theta' \qquad (5)$$

For the direct scattering problem, the scattered field E_s is calculated by assuming that the shape is known. This can be achieved by first solving J in (5) and then calculating E_s using (3).

Let us consider the following inverse problem: given the scattered electric field E_s measured outside the scatterer, determine the shape function $F(\theta)$ of the object.

Numerical Results

We illustrate the performance of the proposed inversion algorithm and its sensitivity to random noise in the scattered field. Consider a lossless three- layer structure ($\sigma_1 = \sigma_2 = \sigma_3 = 0$) and a perfectly conducting cylinder buried in region 2. The permittivity in each region is characterized by $\varepsilon_1 = \varepsilon_0$, $\varepsilon_2 = 2.55\varepsilon_0$ and $\varepsilon_3 = \varepsilon_0$ respectively, as shown in Fig. 1. The frequency of the incident wave is chosen to be 3 GHz, with the incident angles equal to 45° and 315°, respectively. The width of the second layer is 0.3 m. Ten measurement points are equally separated on two parallel lines at equal spacing in region 1 and region 3. Thus there are totally 20

measurements in each simulation. Both two kinds of shape expansion are used in the direct problem. However, only the cubic-spline expand is used for the inverse problem to guarantee nonnegative definitions of the shape.

In both algorithms, the population size are chosen as 100 (i.e. X =100). The binary string length of the unknown coefficient, ρ_i is set to be 20 bits (i.e., L=20). The search range for the unknown coefficient of the shape function is chosen to be from 0 to 0.1. The extreme value of the coefficient of the shape function can be determined by the prior knowledge of the objects. The crossover used by SGA is chosen as 0.8. Note that, in a typical GA, it uses the crossover and mutation operator to generate all the new population in each new generation. On the contrary, NU-SSGA only needs to generate a few new population in each new generation. The mutation probability p_m is set to be 0.1 in both algorithms. The value of β is chosen to be 0.001. The efficient NU-SSGA is then applied to enhance the convergence and increase the converging rate of finding the global extreme of the inverse scattering problems.

In this example, the shape function is selected by the Fourier series as $F(\theta) = 0.03 + 0.006\cos\theta + 0.004\cos 2\theta + 0.005\cos 3\theta$ m and we use cubic-spline expand to recover it. The reconstructed shape function at 6000 function calls using by SGA and NU-SSGA are plotted in Fig. 2(a) respectively with the relative errors shown in Fig. 2(b). It is found that even the description of the shape are different in direct and inverse problems, the NU-SSGA can get the good result in very short time compared to SGA.

Here DR, which is called shape function discrepancy respectively, are defined as

$$DR = \{\frac{1}{N'}\sum_{i=1}^{N'}[F^{cal}(\theta_i) - F(\theta_i)]^2 / F^2(\theta_i)\}^{1/2} \tag{10}$$

where N' is set to 60. The quantities DR provides measures of how well $F^{cal}(\theta)$ approximates $F(\theta)$ respectively. From Fig. 2(a) and Fig. 2(b), it is clear that the efficiency of the NU-SSGA is much better than that of SGA. We can save more than 90% CPU time by using NU-SSGA.
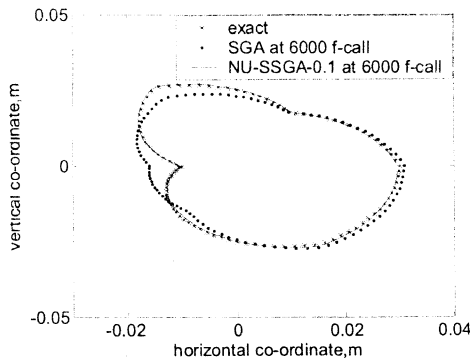

Fig. 2(a) Shape function for example 1. The star curve represents the exact shape, while the curves of dot and solid lines are the results at 6000 function call by using SGA and NU-SSGA-0.1 (crossover=0.1) respectively. respectively.
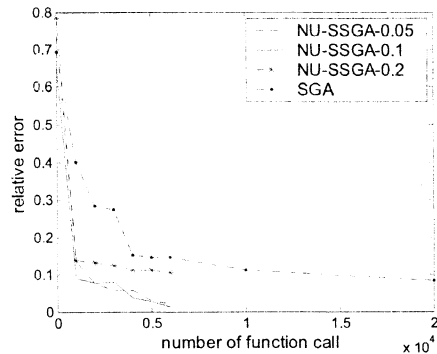
Fig. 2(b) The trend of relative errors for SGA, NU-SSGA-0.05 (crossover=0.05), NU-SSGA-0.1 (crossover=0.1) and NU-SSGA-0.2 (crossover=0.2) methods.

Conclusions

We have presented a study of comparing the efficiency of the SGA and NU-SSGA with different crossover rate to reconstruct the conducting image in a slab medium through knowledge of scattered field. Based on the boundary condition and measured scattered field, we have derived a set of nonlinear integral equations and reformulated the imaging problem into an optimization problem. Besides, the contours of the cylinders are expanded by the cubic-spline for the inverse problem instead of the trigonometric series to guarantee the nonnegative definition of the shape. Experiment results show that the searching ability and efficiency of NU-SSGA depends on the suitable crossover rate. There is no doubt that NU-SSGA will reduce a lot of CPU time in imaging problems. In our experiment results, the best crossover rate in NU-SSGA is 0.1 and we can save more than 90% CPU time to get the satisfied result for all the examples.

References

1. W. Chien, C. C. Chiu and C. L. Li, "Cubic-Spline Expansion with GA for a Conducting Cylinder Buried in a Slab Medium," *Electromagnetics* Vol. 26, No. 5, pp. 329-343, July 2006.
2. J.Michael Johnson and Yahya Rahmat-Samii, "Genetic algorithms in engineering electromagnetics," *IEEE Antennas Propagat. Mag.*, vol.39, pp. 7-21, Aug. 1997
3. C. C. Chiu and P. T. Liu, "Image reconstruction of a perfectly conducting cylinder by the genetic algorithm," *IEE Proc.-Micro. Antennas Propagat.*, vol. 143, pp.249-253, June 1996.